Earth's Future

RESEARCH ARTICLE
10.1029/2023EF003837

Hydroclimatic Vulnerability of Wetlands to Upwind Land Use Changes

Simon Felix Fahrländer[1,2], Lan Wang-Erlandsson[2,3], Agnes Pranindita[3], and Fernando Jaramillo[1,4]

[1]Department of Physical Geography and Bolin Centre for Climate Research, Stockholm University, Stockholm, Sweden, [2]Potsdam Institute for Climate Impact Research (PIK), Member of the Leibniz Association, Potsdam, Germany, [3]Stockholm Resilience Centre, Stockholm University, Stockholm, Sweden, [4]Baltic Sea Centre, Stockholm University, Stockholm, Sweden

Key Points:

- Land use changes have led to mean annual runoff ($P–E$) decreases in wetland hydrological basins globally
- The most substantial land use-related $P–E$ changes occurred in tropical and subtropical wetlands across Asia and South America and in Europe
- We identify eight wetlands in Asia, South America, and Australia as particularly vulnerable to changes in upwind moisture sources

Supporting Information:

Supporting Information may be found in the online version of this article.

Correspondence to:

S. F. Fahrländer,
simon.fahrlaender@pik-potsdam.de

Citation:

Fahrländer, S. F., Wang-Erlandsson, L., Pranindita, A., & Jaramillo, F. (2024). Hydroclimatic vulnerability of wetlands to upwind land use changes. *Earth's Future*, *12*, e2023EF003837. https://doi.org/10.1029/2023EF003837

Received 30 MAY 2023
Accepted 30 JAN 2024

Author Contributions:

Conceptualization: Simon Felix Fahrländer, Lan Wang-Erlandsson, Agnes Pranindita, Fernando Jaramillo
Formal analysis: Simon Felix Fahrländer
Funding acquisition: Fernando Jaramillo
Methodology: Simon Felix Fahrländer
Supervision: Lan Wang-Erlandsson, Fernando Jaramillo
Visualization: Simon Felix Fahrländer
Writing – original draft: Simon Felix Fahrländer
Writing – review & editing: Lan Wang-Erlandsson, Agnes Pranindita, Fernando Jaramillo

Abstract Despite their importance, wetland ecosystems protected by the Ramsar Convention are under pressure from climate change and human activities. These drivers are altering water availability in these wetlands, changing water levels or surface water extent, in some cases, beyond historical variability. Attribution of the effects of human and climate activities is usually focused on changes within the wetlands or their upstream surface and groundwater inputs. However, the reliance of wetland water availability on upwind atmospheric moisture supply is less understood. Here, we assess the vulnerability of 40 Ramsar wetlands to precipitation changes caused by land use and hydroclimatic change occurring in their upwind moisture-supplying regions. We use moisture flows from a Lagrangian tracking model, atmospheric reanalysis data, and historical land use change (LUC) data to assess and quantify these changes. Our analyses show that historical LUC has decreased precipitation and terrestrial moisture recycling in most wetland hydrological basins, decreasing surface water availability (precipitation minus evaporation). The most substantial effects on wetland water availability occurred in the tropic subtropical regions of Central Europe and Asia. Overall, we found wetlands in Central Asia and South America to be the most vulnerable by a combination of LUC-driven effects on runoff, high terrestrial precipitation recycling, and recent decreases in surface water availability. This study stresses the need to incorporate upwind effects of land use changes in the restoration, management, and conservation of the world's wetlands.

Plain Language Summary Wetlands protected by the Ramsar Convention face threats from climate change and human activities, impacting their water availability and altering wetland functions. While past studies often focused on threats from their immediate surroundings, our research looks into the influence of changes in their upwind atmospheric moisture supply. We evaluate the vulnerability of 40 Ramsar wetland basins to precipitation shifts caused by land use and hydroclimatic changes in upwind regions, using the output of an atmospheric moisture tracking model and historical data. The results indicate that historical land use changes have reduced precipitation and moisture recycling, leading to a decrease in water availability in some wetlands, notably affecting tropical and subtropical regions of Central Europe and Asia. We assess that wetlands in Asia and South America face are vulnerable to a combination of land use-induced runoff impacts, high precipitation recycling, and declining surface water availability. This study highlights the need to incorporate upwind effects of land use changes in wetland restoration, management, and conservation efforts globally, recognizing their crucial role for effective strategies for wetland protection amidst evolving environmental conditions.

1. Introduction

Wetlands are responsible for around 45% of all the value generated by natural biomes globally (Davidson et al., 2019) and are critical to the health and livelihoods of many people globally (Ramsar Convention on Wetlands, 2021). They protect coasts and water quality, maintain and regulate groundwater levels and soil moisture, help mitigate floods, sequester carbon, and support impressive biodiversity (Thorslund et al., 2017). These ecosystems are also critical to sustainable development (Jaramillo et al., 2019). However, the provisioning of these services is compromised by low water availability, as impacted by past, ongoing and future land and water management and anthropogenic climate change.

Table 1
Overview of the Digital Elevation Models (DEMs) Used for Hydrological Basin Delineation

Service	Sources	Resolution (m)	Coverage
EU-DEM	ASTER GDEM, SRTM, Russian Topomap	25	Europe > 60N
DEM3	SRTM, ASTER GDEM, Russian 200k and 100k	90	Russia > 60N
SRTM 90m	SRTM	90	Global < 60N
CDED	CCMEO	20	Canada

Note. Acronyms: ASTER, Advanced Spaceborne Thermal Emission and Reflection Radiometer; GDEM, Global Digital Elevation Map; SRTM, Shuttle Radar Topography Mission; CDED, Canadian Digital Elevation Data; CCMEO, Canada Center for Mapping and Earth Observation.

In particular, agricultural expansion (Kashaigili, 2008), fragmentation by road infrastructure (Jaramillo et al., 2018a, 2018b; Wemple et al., 2018), water impoundment (Grill et al., 2019), and freshwater withdrawals for irrigation (Zaki et al., 2020) significantly alter wetland water availability. In addition, climate change also modifies the evaporation and precipitation of wetland systems, leading to drying or wetting (Xi et al., 2021). Since 1970, approximately 35% of global wetland areas have been lost due to local land use conversions and hydrological modifications, such as drainage for agricultural use (Fluet-Chouinard et al., 2023). Although the loss rate has slowed in regions like Europe and North America, it has increased over large parts of Asia and the tropics (Acreman et al., 2007; Davidson, 2016).

Land use changes occurring upstream of the wetland can alter water availability within the wetland ecosystem; changes in vegetation and land use alter land evaporation (i.e., the total of transpiration, soil moisture evaporation, and interception evaporation), modifying the amount and timing of freshwater flowing into the wetland (Sterling et al., 2013). However, upwind land use-induced changes can also modify precipitation over the wetlands' hydrological basin by altering wind patterns and terrestrial moisture recycling (i.e., the process whereby land evaporation is transferred to the precipitation over land; Tuinenburg & Staal, 2020). The impact can be substantial, as 40%–50% of terrestrial precipitation comes from evaporation over land, and 60%–70% of evaporation over land results in terrestrial precipitation (Eltahir & Bras, 1996; Tuinenburg & Staal, 2020; van der Ent et al., 2010). Furthermore, around half of this moisture supply to terrestrial precipitation is sustained by vegetation and can be considered an ecosystem service (Keys et al., 2016). In fact, current human land use covers over 40%–50% of the Earth's land surface (Ellis & Ramankutty, 2008) and is known to already impact precipitation and river flow through modifications of moisture recycling (Wang-Erlandsson et al., 2018).

The upwind area of the most important moisture supply to these wetlands, termed “precipitationshed” (Keys et al., 2012), can then help identify transboundary upwind-downwind moisture transport relationships (Keys et al., 2017; Wang-Erlandsson et al., 2018). Hence, it can also be used to determine the wetlands' vulnerability to upwind land use change (LUC). Although similar upwind vulnerability assessments have been done for megacities (Keys et al., 2018), croplands (Keys et al., 2012), and critical natural assets (Chaplin-Kramer et al., 2022), there is still no assessment of the vulnerability of wetland water availability to upwind changes. Such assessment would provide evidence of the need to incorporate upwind effects of land use changes in the restoration, management, and conservation of the world's wetlands and to evaluate their resilience to human and hydroclimatic changes.

Here, we assess the hydroclimatic vulnerability of 40 wetland hydrological basins to upwind changes in land use when accounting for terrestrial moisture recycling. The hypothesis is that upwind land use changes can drive considerable changes in long-term water availability in the hydrological basins of wetlands. We use a database of atmospheric flows created with the Lagrangian UTrack atmospheric moisture tracking model, atmospheric reanalysis data, and historical LUC data.

2. Methods and Data

2.1. Data

This study uses global land data to describe the characteristics of the selected wetlands of the Ramsar Convention (https://rsis.ramsar.org/?pagetab=1) (Section 2.1.1) and hydrometeorological data to describe their moisture

flows (Section 2.1.2). Information on land includes Digital Elevation Models (DEMs) for basin delineation (see Table 1) and data on current global anthromes to characterize land use from moisture sources (Ellis et al., 2013). Hydrometeorological data include moisture flow data for moisture recycling analyses (Tuinenburg et al., 2020), modelled outputs of evaporation and precipitation for estimating the impact of LUC (Wang-Erlandsson et al., 2018), and precipitation and evaporation data for the moisture recycling and hydroclimatic trend analysis (Hersbach et al., 2020; University of East Anglia Climatic Research Unit et al., 2021).

Since data were accessed from multiple sources with different temporal and spatial scales, resolutions, and metadata, they were pre-processed by transforming, subsetting, and transposing procedures for consistency. This pre-processing of data was done using the open-source and Linux-based command line operators of the Geospatial Data Abstraction Library (Rouault et al., 2022) and Climate Data Operators (Schulzweida, 2020). Next, the gridded data were transposed to match the UTrack climatology data set (Tuinenburg et al., 2020) at 0.5° resolution using the bilinear transposing method and the World Geodetic System 1984 (EPSG:4326) was applied to all geospatial data sets. Finally, Raster and shapefiles were converted with the Python packages geopandas and rasterio (Gillies et al., 2013).

2.1.1. Land Data

Wetland location markers and water body delineations were taken from the Ramsar Convention data set (https://rsis.ramsar.org/) and from Zhang et al. (2017), who used remote sensing to map and classify wetlands of the Ramsar Convention. For the delineation of the basin boundaries of selected wetlands, the water body delineations and several DEMs were used (Table 1). Since some hydrological basins extend beyond the latitude 60° North and global DEMs often exclude these areas, we used additional region-specific models to delineate the northernmost basins in Europe, Canada and Russia. For wetlands in the deltas of major river basins (see Table 2 in Section 2.2.2), the hydrological basin boundaries were taken from the Global Runoff Data Center (GRDC, 2020). Furthermore, optical images from the Google Earth engine were also used to validate and, if necessary, manually adjust the wetland's outlet and generate an accurate boundary.

Furthermore, the Anthropogenic Biomes of the World v2 (year 2000 version) dataset (Ellis et al., 2013) was used to determine the contribution to moisture supply per land use type (Section 2.2.4). This dataset focuses on anthropogenic alterations by global LUC. The 19 anthromes were aggregated into seven categories (i.e., Dense settlements, rainfed cropland, woodland, rice and irrigated cropland, rangeland, and barrenland), following Keys et al. (2012). In addition, we grouped residential, populated, and remote rangelands into a single category, “Rangeland,” by assuming similar hydrological characteristics. Finally, to distinguish between terrestrial and oceanic evaporation sources, a land-sea mask was accessed through the ERA5-Reanalysis Single Levels Data set of the European Center for Medium-Range Weather Forecasts (ECMWF) (Hersbach et al., 2020).

2.1.2. Hydrometeorological Data

We used three hydrometeorological data sets for different purposes: (a) analyzing hydroclimatic trends (Sections 2.2.3 and 3.1), (b) establishing moisture sources and sinks relationships (Sections 2.2.4 and 3.2), and (c) estimating LUC impacts on precipitation (Sections 2.2.5 and 3.3). Subsequently, each contributed to estimating a sub-indicator of vulnerability, used to obtain a final vulnerability indicator (Sections 2.2.6 and 3.4).

First, for analyzing hydroclimatic trends (Section 2.2.3), we used precipitation and evaporation data from the CRU-TS4.05 monthly data set from 1980 to 2020 (Harris et al., 2020). The data set was used to determine water availability in the hydrological basins and their change over time. The CRU-TS version 4 data set is a global climate data set derived through interpolating observation data, which are better suited for calculating hydroclimatic trends than reanalysis as they are constructed based on observations (Jaramillo & Destouni, 2014).

Second, for moisture recycling analyses (Section 2.2.4), we used the output of the Lagrangian atmospheric moisture tracking model UTrack (Tuinenburg et al., 2020; see Supporting Information S1). This global data set contains the mean monthly moisture flows from 2008 to 2017 between each pair of moisture source and sink cells. For every grid cell in the world, the data set provides the fraction of upwind evaporation from each source cell that contributes to its precipitation. The moisture tracking of UTrack was initially performed at 0.25°-resolution and 0.1-hr timesteps using hourly atmospheric reanalysis data from the ECMWF Reanalysis v5 (ERA5) data set (wind and specific humidity at 25 pressure levels and surface data of land and ocean evaporation and precipitation)

Table 2
List of the 40 Selected Wetlands With Abbreviated Names, Ramsar Identification Number, Country, Continent and Surface Area According to Ramsar (km^2)

No	Name	Abbreviation	Ramsar ID	Country	Continent	Area (km^2)
1	Chott Ech Chergui	Chergui	1052	Algeria	Africa	8,555
2	Basse Valée de l'Ouémé	Ouémé	1018	Benin	Africa	6,528
3	Okavango Delta System	Okavango	879	Botswana	Africa	55,374
4	Plaines d'inondation du Chad	Plaines	1839, 1560, 1621	Chad	Africa	104,269
5	Grands affluents & Ngiri-Tumba-Maindombe	Ngiri	1742, 1784	Congo, DRC	Africa	124,777
6	Bassin de la Lufira	Lufira	2318	DRC	Africa	44,710
7	Sankarani-Fié	Sankarani	1167	Guinea	Africa	16,560
8	Delta Intérieur du Niger	Niger	1365	Mali	Africa	41,195
9	Zambesi Delta	Zambesi	1391	Mozambique	Africa	31,712
10	Sudd	Sudd	1622	South Sudan	Africa	57,000
11	Dalai Lake National Nature Reserve, Inner Mongolia	Dalai	1146	China	Asia	7,400
12	Sichuan Changshagongma Wetlands	Sichuan	2348	China	Asia	6,698
13	Tibet Selincuo Wetlands	Tibet	2352	China	Asia	18,936
14	Ili River Delta and South Lake Balkhash	Ili	2020	Kazakhstan	Asia	9,766
15	Indus Delta	Indus	1284	Pakistan	Asia	4,728
16	Volga Delta	Volga	111	Russia	Asia	8,000
17	Tobol-Ishim Forest-steppe	Tobol	679	Russia	Asia	12,170
18	Parapolsky Dol	Parapol	693	Russia	Asia	12,000
19	Brekhovsky Islands in the Yenisei estuary	Yenisei	698	Russia	Asia	14,000
20	Coongie Lakes	Coongie	376	Australia	Australia	21,790
21	Kakadu National Park	Kakadu	204	Australia	Australia	19,798
22	Sian Ka'an	Sian	1329	Mexico	Central America	6,522
23	Rio Sabinas	Sabinas	1769	Mexico	Central America	6,031
24	Lemmenjoki National Park	Lemmen	1521	Finland	Europe	2,860
25	Etangs de la Champagne humide	Etangs	514	France	Europe	2,558
26	Danube Delta	Danube	521	Romania	Europe	6,470
27	Donana National Park	Doñana	234	Spain	Europe	1,116
28	Sjaunja	Sjaunja	32	Sweden	Europe	1,813
29	Whooping Crane Summer Range	Crane	240	Canada	North America	16,895
30	Queen Maud Gulf	Maud	246	Canada	North America	62,782
31	Dewey Soper Migratory Bird Sanctuary	Dewey	249	Canada	North America	8,159
32	Polar Bear Provincial Park	Bear Park	360	Canada	North America	24,087
33	Everglades National Park	Everglade	374	USA	North America	6,105
34	Banados del Río Dulce y Laguna de Mar Chiquita	Dulce	1176	Argentina	South America	9,960
35	Los Lípez	Lipez	489	Bolivia	South America	14,277
36	Río Blanco	Blanco	2092	Bolivia	South America	24,049
37	Ilha do Bananal	Bananal	624	Brazil	South America	5,623
38	Rio Negro	Negro	2335	Brazil	South America	120,016
39	Pantanal	Pantanal	602, 1089	Brazil, Bolivia	South America	33,249
40	Pacaya-Samiria & Complejo de humedales del Abanico	Pacaya	546, 1174	Peru	South America	59,073

Note. Four of the study sites are an aggregate of multiple Ramsar Sites; for example, Wetland Nr. 2 sums three floodplains in Chad, Nr. 5 aggregates the Grands affluents and Ngiri-Tumba-Maindombe wetlands in Congo and the Democratic Republic of the Congo, Nr.40 includes the Pacaya-Samiria wetlands and Complejo de humedales del Abanico in Peru, and Nr. 39 combines the Bolivian and Brazilian sections of the Pantanal wetland.

(Hersbach et al., 2020). The UTrack modelled data was later aggregated to a monthly resolution and an output of 0.5° and 1° spatial resolution, of which we used the former. As monthly resolution of the data set limits the understanding of moisture dynamics arising from shorter climatic events, such as those linked with typhoons and hurricanes, resolving moisture supply to wetlands based on these climatic events is beyond the scope of this study (Wang et al., 2016). Monthly evaporation and precipitation data from ERA5 from 2008 to 2017 were further processed to agree with the mean monthly moisture flows of the UTrack output (Tuinenburg et al., 2020).

Third, to assess the implications of LUC, we used evaporation and precipitation model outputs for current and potential vegetation scenarios (Section 2.2.5). This data set was taken from the two-way coupled model runs between the hydrological model STEAM and the moisture recycling model WAM-2layers described in Wang-Erlandsson et al. (2018) in 1.5° × 1.5° spatial resolution covering the period from 2000 to 2013.

2.2. Methods

2.2.1. Summary of the Methods

The main workflow of the methods is the following. First, we selected and delineated 40 wetlands of the Ramsar Convention which could give a global representation in terms of size and location (Section 2.2.2). We calculated precipitation (P) and water availability (i.e., $P–E$) over the wetland's hydrological basin and their trends in time (Section 2.2.3). Second, we estimated the moisture supply to these wetland hydrological basins using moisture flow trajectories from the UTrack model (Tuinenburg et al., 2020) and computed their precipitationsheds (Section 2.2.4). Hence, we estimated terrestrial (ρ_{terr}) and basin internal moisture (ρ_{int}) recycling ratios for each wetland hydrological basin. Third, we isolated the impact of vegetation changes on moisture supply in the form of precipitation to the wetland hydrological basins by pairing the moisture tracking with the (a) current land use classification (Ellis et al., 2013; Wang-Erlandsson et al., 2018) and (b) potential vegetation scenarios data set (Wang-Erlandsson et al., 2018) (Section 2.2.5). From here on, we obtained the precipitation and evaporation for both scenarios, P_{cur} and E_{cur} and P_{pv} and E_{pv}, respectively, and calculated their difference (i.e., current minus potential) for P, $P–E$, and ρ_{terr}. Finally, the vulnerability (VI) of the wetlands to upwind moisture supply changes linked to LUC was estimated based on the observed recent hydroclimatic changes, LUC impacts on water availability and terrestrial precipitation recycling (Section 2.2.6).

2.2.2. Wetland Selection and Delineation

Forty wetlands of international importance (Table 2) were selected to obtain balanced global coverage and ensure a reliable output from the soil moisture tracking algorithm; we focused on wetlands with an area greater than 2,000 km^2. In Europe, where Ramsar wetlands are smaller than elsewhere, the minimum size was set instead to 1,000 km^2 to include representative wetlands such as Doñana National Park in Southern Spain and the Sjaunja Wetlands in Northern Sweden. The subset of wetlands meeting these criteria includes 10 wetlands in Africa, nine in Asia and South and Central America, five in Europe and North America and two in Australia. The selection comprises different wetland types, including peatlands (e.g., Polar Bear Provincial Park, Queen Maud Gulf), river floodplains (e.g., Grands affluents, Rio Negro), mountainous headwater wetlands (e.g., Sichuan Changshagongma Wetlands), coastal wetlands (e.g., Sian Ka'an, Everglades), and wetlands located around lakes (e.g., Coongie Lakes) and river deltas (e.g., Indus delta, Zambesi delta).

The hydrological basins of the 40 wetlands were delineated in ArcMap using the ArcGIS Spatial Analyst Hydrology Toolbox. Since the entire hydrological basin upstream of the wetland contributes to the surface water inputs to each wetland, the hydrological basins were used as sink areas for the moisture tracking process.

2.2.3. Hydroclimatic Trends

The trend in water availability in a given wetland hydrological basin elucidates whether a wetland is historically susceptible to decreasing water influxes. We used mean annual $P–E$ as a proxy for water availability, as it relates to the amount of water that runs on the surface and is potentially stored in ground and surface water bodies. We applied the non-parametric Mann-Kendall test for trend analysis (see Supporting Information S1).

Table 3
Moisture Tracking Routines in This Study

Run number	Run name	Input	Output/Objective
Establishing moisture sources (Section 2.2.4)			
1	Base run	ERA5 evaporation and precipitation	Wetland moisture imports climatologically (Figures 2 and 3)
2	LC classification run	ERA5 evaporation and precipitation + Anthromes	Wetland moisture imports by land use type (Figure 4)
LUC impact estimation (Section 2.2.5)			
3	STEAM current land use (incl. irrigation)	STEAM current land use evaporation and ERA-I precipitation	Wetland moisture imports under current land use conditions (Figure 5)
4	STEAM-WAM2layers potential vegetation	STEAM-WAM2layers potential vegetation evaporation and precipitation	Wetland moisture imports under potential vegetation conditions (Figure 5)

Note. Runs 1 and 2 are based on ERA5 inputs (Section 2.1.2) and are used to identify the moisture sources of the wetland basins. Run 2 is combined with the Anthromes data set to link moisture sources to a specific land cover classification. Runs 3 and 4 estimate the impact of LUC based on the STEAM-WAM-2layers evaporation and precipitation scenarios for current land use and potential vegetation, respectively (Section 2.1.2).

2.2.4. Establishing Moisture Sources

To "backtrack" the precipitation in the sink (wetland basins) to its sources of evaporation (precipitationsheds), we used the moisture flow database and method created and described by Tuinenburg et al. (2020) (see Section 2.1.2). The process is called "offline" tracking because the data set only supplies monthly averaged atmospheric trajectories, not re-calculating them for every timestep. Although the database shows moisture flows in both directions (source to sink and vice-versa), it is based on forward simulations of evaporation in a source cell to its sink cells. Hence, to extract correct backward flows, forward tracking from each possible source cell for each sink cell in a sink region has to be performed individually and eventually summed up. To avoid the large computational requirements needed to use this method on all the hydrological basins, we used the forward tracking method suggested by Tuinenburg et al. (2020) in the backward direction. We multiplied the resulting normalized evaporation source arrays by the specific precipitation from the sink cells, adding these backward footprints of precipitation up for each sink region. This way, the sink regions tracked precipitation is equal to ERA5 precipitation, while the cellwise contributions of evaporation are still accurately represented. It is worth mentioning that this does not eliminate the up to 5% error introduced in creating the data set by converting float to integers.

The moisture tracking simulations encompassed four distinct tracking runs (Table 3). The first run (Run 1) employed ERA5 inputs to identify moisture sources for the wetland basins. The second run (Run 2) decomposed the moisture supply to each wetland into their components regarding the land cover at the source (i.e., anthromes). Runs 3 and 4 estimate the impact of LUC on evaporation and precipitation for current land use and potential vegetation scenarios.

The fraction of precipitation over wetland basins that originates from land evaporation is termed terrestrial precipitation recycling ratio (ρ_{terr}) (Equation 1) and was calculated as follows (van der Ent et al., 2010):

$$\rho_{\text{terr}}(x,y) = \frac{P_{E_{\text{terr}}}(x,y)}{P_{\text{total}}(x,y)} \tag{1}$$

where $P_{E\text{terr}}$ denotes the precipitation over a wetland basin (x, y) originating from land evaporation, and P_{total} denotes the total precipitation over the wetland basin (L T^{-1}).

Next, we calculated the internal precipitation recycling ratio (ρ_{int}) (Equation 2), which refers to the fraction of precipitation over a wetland basin (x,y) originating from evaporation in the same basin.

$$\rho_{\text{int}}(x,y) = \frac{P_{E_{(x,y)}}(x,y)}{P_{\text{total}}(x,y)} \tag{2}$$

For each wetland hydrological basin, we estimated the 70%-precipitationsheds, that is, the upwind area that contributes 70% of the total precipitation in the sink region (Keys et al., 2012). The precipitationshed is delineated

based on grid cells ranked from high to low moisture contribution to the sink region, thereby excluding the areas with the weakest contributions of evaporation. An important difference between the wetland hydrological basins and the precipitationsheds is the non-stationarity and the more probabilistic nature of the latter. For instance, moisture flows and atmospheric transport patterns are mainly defined by wind speeds, atmospheric pressure, and other atmospheric parameters with vertical as well as horizontal variability (see modeling approaches by Tuinenburg and Staal (2020) and van der Ent (2014)). However, Keys et al. (2014) also state that precipitationsheds can be persistent in the long term, allowing the concept to be used to investigate precipitation sources of specific sink regions.

Next, we overlaid the moisture data with the Anthromes Biome Classification. We aggregated the volumetric precipitation per land use type to calculate the moisture contribution per land use type within the precipitationshed to the total precipitation in the hydrological basin. The land-sea mask, the biome classification, and the precipitationshed datasets were transposed to the same geographical coordinates for this task.

2.2.5. Land Use Change Impacts

To analyze the impact of LUC on wetland basins, we reran the moisture tracking with evaporation and precipitation data under current land and a potential vegetation scenario (Table 3). Run 3 utilizes the STEAM evaporation and precipitation for current land use, including irrigation. In contrast, Run 4 explores potential vegetation conditions (Section 2.1.2). The outcomes of these runs provide insights into wetland moisture imports under current and potential future land use scenarios, as illustrated in Figure 5.

We calculated P, $(P–E)$ and ρ_{terr} for both scenarios and subtracted the results of the potential vegetation scenario from the results of the current vegetation scenario, with a negative value indicating a decrease in $(P–E)$ and ρ_{terr} caused by land use changes and positive value an increase.

2.2.6. Wetland Vulnerability Classification

We introduced a vulnerability index (VI) to define the wetland's hydroclimatic vulnerability. The index is only meant to account for water availability impacts, meaning that only a decrease in water availability is considered a problem. The VI is based on the dependence of the wetland hydrological basin on terrestrial evaporation to sustain its precipitation and ranges from 0 to 3, where higher values imply a higher vulnerability. It is calculated as follows.

$$\text{VI} = \left[1 - \Delta(P-E)_n\right] + \left[1 - \left(\Delta(P_{\text{cur}} - E_{\text{cur}}) - \Delta(P_{\text{pv}} - E_{\text{pv}})\right)_n\right] + \rho_{\text{terr}} \quad (3)$$

where $\Delta(P-E)_n$ is the normalized hydroclimatic trend (Section 2.2.3), the term $\left(\Delta(P_{\text{cur}} - E_{\text{cur}}) - \Delta(P_{\text{pv}} - E_{\text{pv}})\right)_n$ is the normalized difference of water availability between the potential vegetation and current land use scenarios (Section 2.2.5), and n indicates that the values are normalized between 0 and 1. Finally, ρ_{terr} is the terrestrial precipitation recycling ratio over the basins (Section 2.2.4).

3. Results

3.1. Hydroclimatic Trends

The hydroclimatic trends analysis indicates that surface water availability, here expressed as $P–E$, has decreased in the hydrological basins and precipitationsheds of wetlands in Eurasia and the southern half of South America (Figure 1). On the other hand, it has increased across Africa and the Amazon. Consistent significant trends across hydrological basins and precipitationsheds occur for the wetlands of Dulce in South America, Etangs in Europe, Dalai in Asia and Niger and Sankarani in Africa, with the first two experiencing the largest decreases in water availability among the selected wetlands. We generally find significant $P–E$ trends (Mann-Kendall, $p < 0.05$) in 14 hydrological basins and 11 precipitationsheds. For instance, $P–E$ increases significantly in the Bear Park, Tibet, Plaines, Sudd, Niger, Lufira, Sankarani and Everglades wetland hydrological basins, while it decreases in Dalai, Dewey, Dulce, Bananal, Blanco, and Etangs. Additional analysis of the individual trends of P, ET and aridity can be found in Supporting Information S1 (Figures S1–S3 in Supporting Information S1).

10.1029/2023EF003837

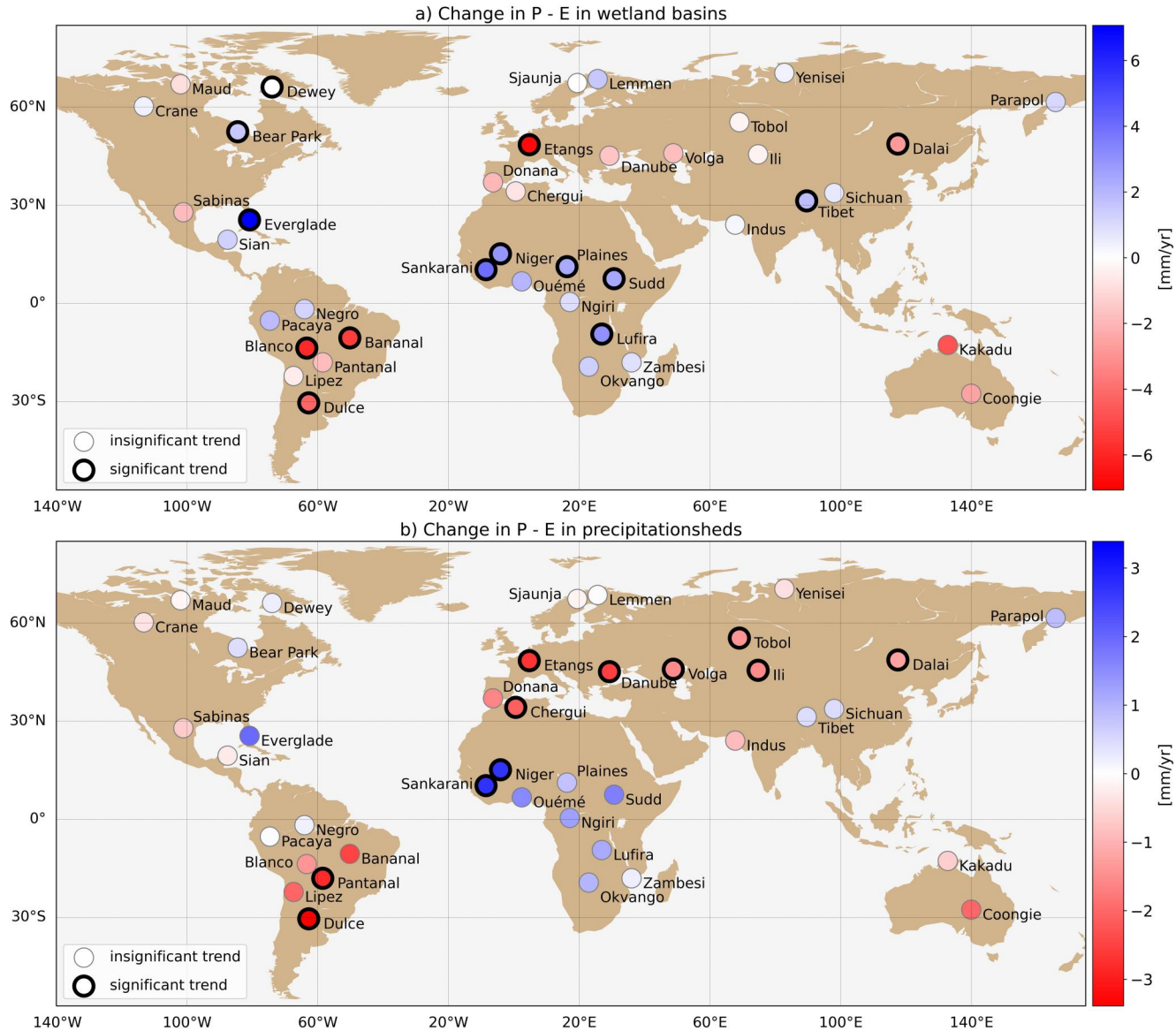

Figure 1. Trends in mean annual precipitation minus evaporation (*P*–*E*) in mm/year during the period 1980–2020 for the set of (a) wetland hydrological basins and (b) their precipitationsheds, calculated from CRU-TSv4.05 precipitation and evaporation using the Mann-Kendall test (Sen-slope). Significant trends (p-value < 0.05) are highlighted with black rings.

3.2. Upwind Moisture Sources to Precipitation in Wetlands Basins

The upwind areas providing moisture for precipitation in the hydrological basins of the 40 wetlands, termed precipitationsheds, cover a large part of the global terrestrial surface (Figure 2). Overall, 45% of the area of the precipitationsheds is terrestrial, and 55% oceanic, with their areas often transgressing national boundaries and covering both oceanic and terrestrial regions. For example, while the precipitationshed of the Canadian wetlands covers most of North America, precipitation for the wetlands in Mexico (Sian and Sabinas Nr. 22 and Nr. 23) and the Everglades in Florida (Nr. 33) originate on the Mexican mainland, the coastal Pacific, the Caribbean Sea and the Atlantic Ocean. Furthermore, while the South American wetlands (i.e., Nr. 34–40) draw moisture from the South American land surface and the equatorial and subequatorial Atlantic, the African wetlands (e.g., Nr. 2–10) receive moisture mainly from Sub-Saharan Africa, the tropical Atlantic Ocean and the oceanic strip along the eastern African coast. Regarding European and West Asian wetlands, there is a considerable overlap of moisture

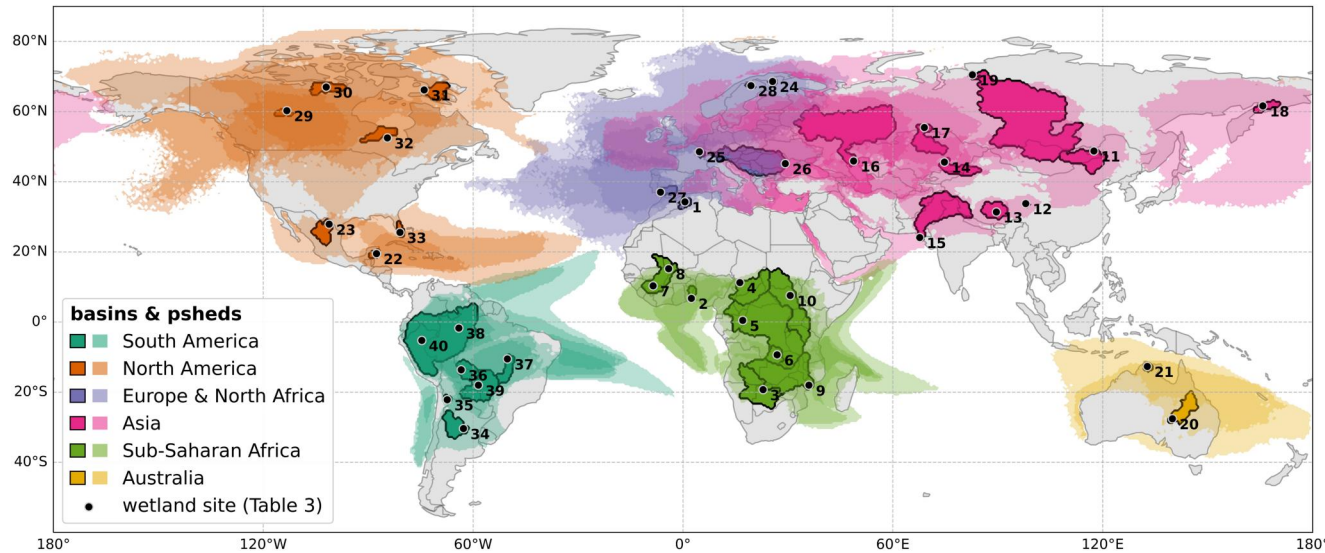

Figure 2. The 70%-precipitationsheds (transparent) and hydrological basins (colored and black boundaries) of the 40 Ramsar wetlands (black dots), based on the "Base run" using ECMWF Reanalysis v5 reanalysis data (see Table 3). The color scheme portrays the studied basins and their precipitationsheds in different colors according to their regions to highlight the regionality of the precipitation sources. See Supporting Information S1 for a more detailed mapping of hotspot wetlands.

sources, with some depending on moisture from the European land surface and even from parts of the North Atlantic.

Generally, wetlands with higher terrestrial precipitation recycling ratios are concentrated in Africa, South America, and Asia, ranging from 27% (Chergui) to 98% (Sichuan) (Figure 3a). For 23 of the 26 studied wetlands in Africa, South America and Asia, more than half of their precipitation originates from land evaporation. Terrestrial precipitation recycling ratios below 50% are only found in the hydrological basins of Chergui in Africa, Parapol in Asia, and Negro in South America. Conversely, low terrestrial precipitation recycling ratios are found in wetland basins around the Caribbean and Mediterranean Seas and Australia. Regarding internal precipitation recycling, most wetland hydrological basins in North America, Australia and Europe have ratios below 5%, except for that of the Sabinas wetland in Mexico and the Danube delta in Romania, with 8% and 17%, respectively (Figure 3b). The wetland hydrological basins in Asia exhibit ratios ranging from 2% (Sichuan) to 27% (Tibet), suggesting that at most a quarter of the moisture can originate within the wetland hydrological basin. Finally, there appears to be no particular correlation between internal and terrestrial precipitation ratios across the set of wetlands (see Figure S4 in Supporting Information S1).

Regarding the source of moisture for the hydrological basins of these Ramsar wetlands, rangelands are the main upwind contributor of moisture (via evaporation) to precipitation (Figure 4). Woodlands, rainfed cropland and barren lands follow in their magnitude of contribution. It is also worth noting that for some wetlands, such as those of the Indus, evaporation from rice and irrigated cropland can contribute up to 20% of annual precipitation. On the other hand, the contribution of evaporation from dense settlements is negligible. Interestingly, the wetlands with the largest percentage of woodlands over their precipitationsheds, Pacaya, Negro and Blanco in South America, contribute the largest volumetric moisture supply by evaporation as a percentage of total precipitation per year.

3.3. Land Use Change Impacts on Wetland Precipitation and Runoff

The conversion from the potential to the current land cover has resulted in a decrease in precipitation from terrestrial resources (Figure 5a), accompanied by a similar decrease in terrestrial precipitation recycling ratios (Figure 5c) for the case of the wetlands in Europe (e.g., Etangs, Danube, Volga), East Asia and South America (e.g., Pantanal, Blanco). The decrease in total precipitation from converting potential vegetation to current land use is more pronounced for Central Africa and Asia wetlands, such as the Indus, Tibet, Niger and Plaines.

Notably, for 18 of the wetlands, the change in precipitation is accompanied by an opposite change in $P–E$ (Figure 5). Change from potential to current land use decreased precipitation and increased $P–E$ in most wetland

10.1029/2023EF003837

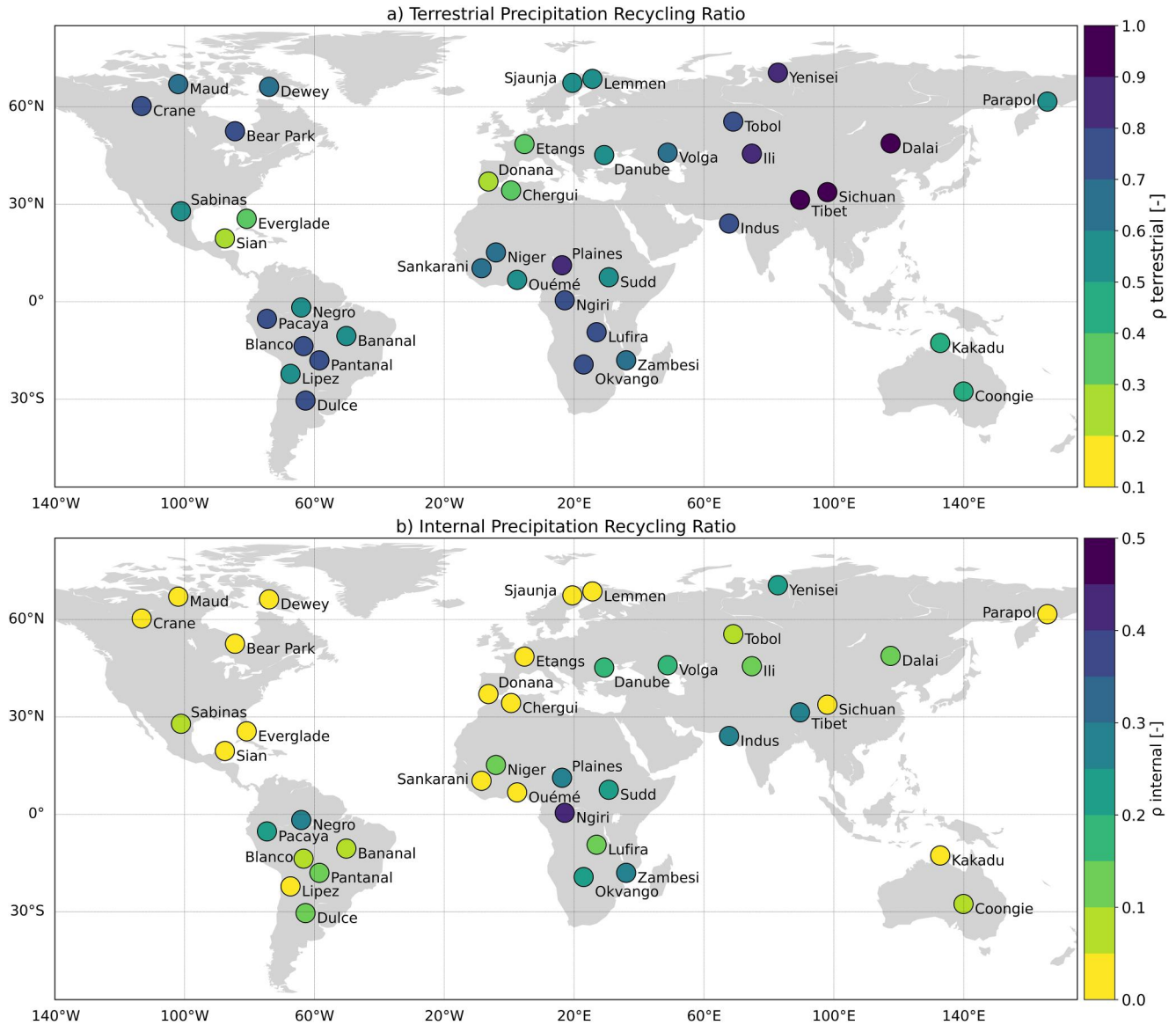

Figure 3. (a) Terrestrial (ρ_{terr}) and (b) internal (ρ_{int}) precipitation recycling ratios for the studied wetland hydrological basins calculated from UTrack backtracking and using Equations 1 and 2, based on the "Base run" using the ECMWF Reanalysis v5 reanalysis data (see Table 3).

hydrological basins (Figures 5a and 5b). On the other hand, the largest precipitation increase occurred for the Indus wetland hydrological basin, gaining ~18 mm/year or a 3% increase in total precipitation. Likewise, the most significant decrease in P occurred in the Danube wetland hydrological basin, where the most substantial reductions in terrestrial recycling have also occurred (Figure 5c). The hydrological basins of Sjaunja, Coongie, Lipez, Yenisei, Sian, Lemmen, Negro experienced a decrease in total P and $P–E$ while Chergui, Sankarani, Niger, Sabinas, Plaines, Ili Tibet and Sichuan present increases in both.

Overall, precipitation over the wetland hydrological basins is affected by LUC, with only six wetlands presenting negligible precipitation changes. However, the relationship between total precipitation and terrestrial changes does not apply to all hydrological basins. Sankarani, for example, shows a decrease in terrestrial precipitation and runoff but a slight increase in the terrestrial precipitation recycling ratio.

10.1029/2023EF003837

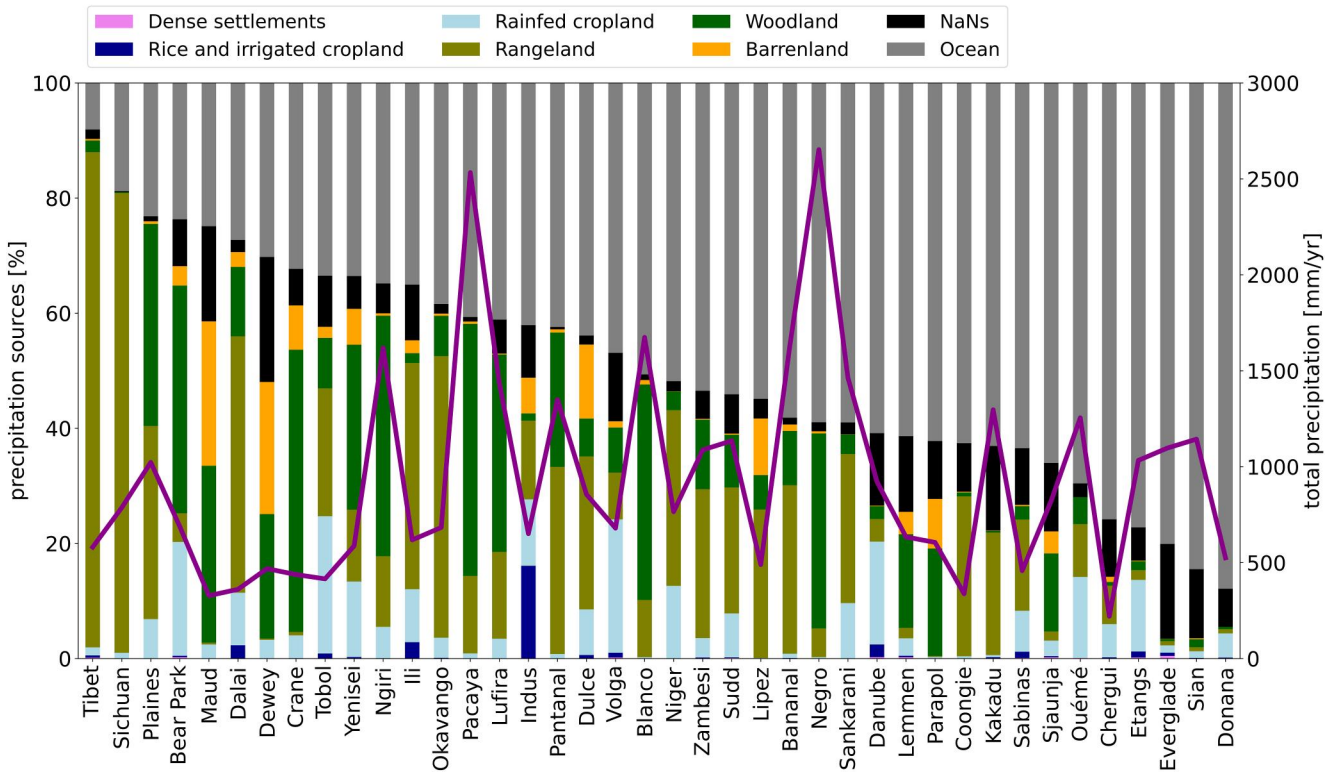

Figure 4. Origin of moisture supply to the wetlands' hydrological basins. Land use contributions of volumetric moisture supply by evaporation, in % of total precipitation per year (left axis and bar plots) and total precipitation to the hydrological basin in mm/year (right axis and red line). Wetlands are sorted based on the volume of terrestrial precipitation recycling, and the LC classification is run using ECMWF Reanalysis v5 reanalysis data and the Anthromes classification (see Table 3).

3.4. Wetland Vulnerability

We assume that the moisture supply of wetlands is hydroclimatically vulnerable when: (a) there is a recent decreasing trend in *P–E* in their hydrological basins and precipitationsheds, (b) their hydrological basins have high terrestrial precipitation recycling ratios and (c) when subject to decreasing *P–E* resulting from upwind LUC. The resulting ranking of vulnerability for all wetlands in Table 4 shows that the most vulnerable wetlands are in Central Asia and South America, with other considerable cases found in Europe (e.g., Danube and Etangs) and Africa (e.g., Ouémé). The moisture supply of many of these relies on evaporation from high-intensity farming lands (e.g., Danube, Volga, Etangs) or high-evaporation tropical ecosystems such as Amazon and Central Africa (Dulce, Pantanal, Ouémé). The precipitationsheds of the first eight "hotspot" wetlands can be seen in Figure S5 in Supporting Information S1. On the other hand, the wetlands at the bottom of the table with low VI indexes are the most resilient to upwind land use and climatic changes, since most upwind moisture originates in the oceans, there is no recent decrease in *P–E,* and land conversion has not resulted in a large change in *P–E*.

4. Discussion

The subsequent three sections discuss the results with a focus on terrestrial precipitation recycling (Section 4.1), LUC and hydroclimatic changes (Section 4.2) and lastly, the limitations of this study (Section 4.3).

4.1. Terrestrial Precipitation Recycling

Wetland basins with high terrestrial precipitation recycling ratios are mostly found in Central Asia, South America, Sub-Saharan Africa and northern Canada. Part of these clusters can be explained by mountain ranges or general wind patterns. Mountain Ranges like the Andes, the Tibetan Plateau and the Great Rift Valley can trap moisture on continents or shield them from the oceans (van der Ent, 2014). For instance, the orographic effect explains the higher terrestrial precipitation recycling in the hydrological basins closer to the East side of the Andes. Conversely, the hydrological basins further away from the Andes or on its West side have slightly lower

10.1029/2023EF003837

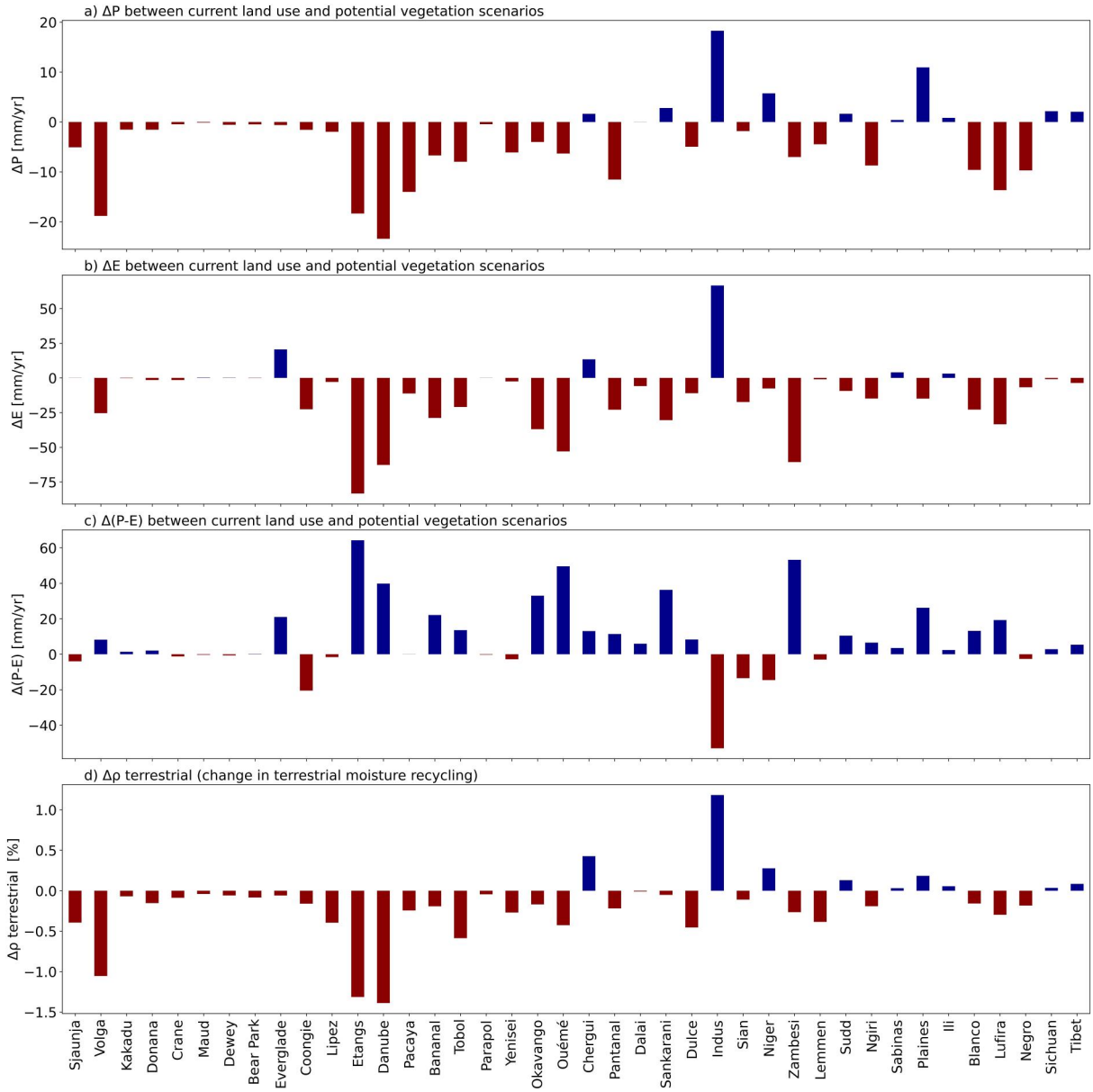

Figure 5. Differences in (a) precipitation (ΔP), (b) evaporation (ΔE), (c) $\Delta(P–E)$ and (d) terrestrial recycling ($\Delta\rho_{terr}$) assuming changes from potential vegetation to current land use for each wetland hydrological basin and based on the "STEAM current and potential LC runs" using STEAM evaporation and precipitation based on current and potential land cover (see Table 3).

terrestrial precipitation recycling ratios. The Tibetan Plateau also keeps moisture over the continent, as seen in the wetland hydrological basins in Tibet and China, which show the highest terrestrial recycling in this study. In Africa, the Great Rift prevents moisture from entering the Indian Ocean in the East (van der Ent, 2014), explaining the high terrestrial recycling in its West. Generally, most tropical continental wetlands also show terrestrial recycling ratios above 50% since shorter distances of atmospheric transport tend to favor higher moisture recycling rates (van der Ent et al., 2014; van der Ent & Savenije, 2011).

Wetland basins with low recycling ratios are mostly found in dry and coastal hydrological basins around the Gulf of Mexico, Europe, and Australia. In these areas, much of the precipitation stems from evaporation over the ocean. For example, the hydrological basins in Florida and Mexico are almost surrounded by oceans and mainly depend on evaporation from the Pacific, the Gulf of Mexico, the Atlantic, and the Caribbean to sustain their precipitation. The hydrological basins in Europe and Northern Africa also strongly rely on moisture from the

Table 4
Wetland Upwind Moisture Vulnerability Index (VI; [Min: 0, Max: Orange]) Based On 1980–2020 Data

Continent	Name	Ramsar ID	Sub-indicator 1 $(P–E)_{\text{trend 1980–2020}}$ (mm/year) (CRU-TS v4.05)	Sub-indicator 2 $(P–E)_{\text{cur}} - (P–E)_{\text{pv}}$ (mm/year) (STEAM—WAM-2layers output)	Sub-indicator 3 ρ_{terr} (ERA5)	Vulnerability indicator VI
Africa	Chergui	1052	−2.1	13.1	0.3	1.6
	Plaines	1839	0.8	26.2	0.9	1.5
	Ngiri	1742	1.3	6.6	0.7	1.4
	Lufira	2318	1.1	19.3	0.7	1.4
	Niger	1365	2.7	−14.6	0.6	1.3
	Okavango	879	1.0	33.0	0.7	1.3
	Sudd	1622	1.7	10.5	0.5	1.2
	Zambesi	1391	0.2	53.2	0.6	1.1
	Ouémé	1018	1.6	49.6	0.5	0.9
	Sankarani	1167	2.7	36.3	0.6	0.8
Asia	Indus	1284	−0.9	−53.0	0.8	2.4
	Dalai	1146	−1.2	5.9	1.0	2.1
	Ili	2020	−1.5	2.4	0.9	2.1
	Yenisei	698	−0.4	−2.8	0.8	1.9
	Sichuan	2348	0.5	2.9	1.0	1.9
	Tobol	679	−1.4	13.6	0.8	1.9
	Tibet	2352	0.4	5.4	1.0	1.8
	Volga	111	−1.5	8.2	0.6	1.8
	Parapol	693	0.9	−0.2	0.5	1.3
Australia	Coongie	376	−2.0	−20.5	0.3	1.8
	Kakadu	204	−0.6	1.4	0.3	1.4
Europe	Danube	521	−2.5	39.8	0.5	1.6
	Lemmen	1521	0.1	−3.0	0.5	1.5
	Sjaunja	32	−0.1	−3.9	0.5	1.5
	Doñana	234	−1.6	2.1	0.2	1.4
	Etangs	514	−2.7	64.3	0.3	1.2
North America	Crane	240	−0.4	−1.2	0.7	1.7
	Maud	246	−0.1	−0.3	0.7	1.7
	Bear Park	360	0.4	0.2	0.7	1.7
	Dewey	249	0.2	−0.6	0.7	1.6
	Sabinas	1769	−0.7	3.5	0.4	1.5
	Sian	1329	−0.3	−13.4	0.2	1.3
	Everglade	374	2.0	21.0	0.2	0.7
South America	Dulce	1176	−3.4	8.3	0.7	2.2
	Pantanal	1089	−2.8	11.4	0.8	2.1
	Lipez	489	−2.0	−1.6	0.5	1.8
	Blanco	2092	−1.4	13.2	0.7	1.8
	Bananal	624	−2.5	22.1	0.5	1.7
	Pacaya	546	0.03	0.04	0.7	1.7
	Negro	2335	0.2	−2.6	0.5	1.5

Note. The table includes Sub-indicator 1; the trend in *P–E* (Sen-slope; min: red, 0: white, max: blue) calculated with CRU-TS v4.05; Sub-indicator 2; the trend of *P–E* change between the potential vegetation and current land use ($\Delta(P–E)_{\text{cur–pv}}$; min: red, 0: white, max: blue) based on land use scenario outputs of STEAM—WAM-2layers (Wang-Erlandsson et al., 2018); and Sub-indicator 3; the terrestrial precipitation recycling ratio based of base run using ERA5 reanalysis (ρ_{terr}: 0: white, 1: green).

Atlantic Ocean, with precipitationsheds reaching far over the Northern Atlantic. The two Australian hydrological basins are also largely dependent on precipitation from the oceans surrounding the Australian continent.

A combination of a high terrestrial and low internal precipitation recycling ratio implies a higher vulnerability of basin water availability to LUC. For some wetland hydrological basins, there is no correlation between terrestrial precipitation recycling and internal basin recycling (e.g., Sichuan and Crane; Figure 3). However, the hydrological basin area and the internal recycling ratio are indeed strongly correlated. The largest wetland hydrological basins are usually the hydrological basins of wetlands located downstream of major river hydrological basins, such as delta wetlands (e.g., Yenisei, Zambesi and Indus) and floodplain wetlands (e.g., Negro, Ngiri, Plaines), which have the highest internal recycling ratios. This makes them less vulnerable to land use changes in terms of their runoff ($P - E$) since possible precipitation and evaporation changes coincide when considering the simplest version of the water balance ($Q = P - E$). When E changes, P is assumed to change similarly, which would result in little to no change in runoff. Wetlands with hydrological basins with high terrestrial recycling and low internal recycling such as the headwater Sichuan and Lipez wetlands strongly depend on terrestrial evaporation from outside their hydrological basin. This implies that upwind changes in climatic conditions and land use may affect moisture supply to these hydrological basins. Here, the implications of such land-atmosphere feedback may be less direct than those caused by local changes in the hydrological basins.

4.2. Land Use and Hydroclimatic Change

Background climate variation alone can partly explain wetland water availability due to the strong influence of Earth's surface air temperatures and precipitation on surface water (Osland et al., 2016; Stagg et al., 2019; Woolway et al., 2020). Nevertheless, the dominant influence of anthropogenic activities cannot be discarded (Wine & Davison, 2019). The current and potential land and vegetation cover in the precipitation areas shed light on the likelihood of potential land use changes and their implications for wetland moisture supply. For instance, if the precipitationshed of a wetland is covered by wooded vegetation that may eventually be converted to cropland or other short vegetation types, then this constitutes a potential vulnerability. In precipitationsheds occupied by croplands and rangelands, negative human impacts on wetland moisture supply have already occurred. However, further degradation due to land cover change is still possible. To reduce the vulnerability of many of the studied wetlands, prevention of further degradations of human-dominated areas is most relevant, since rangelands, woodlands and agricultural lands contribute the most as precipitation sources (in terms of volume of evaporation).

Rangelands are an important precipitation source for the wetland hydrological basins in Australia, Central and East Asia (Tibet, China, Mongolia), and the wetlands whose hydrological basins fall outside of tropical Africa and South America. In addition, the conversion of woodlands to rangelands may inflict additional changes in evaporation (Milton & Siegfried, 1994). Hence, areas where rangelands are expanding or degrading run the risk of causing local and downwind precipitation changes (Keys et al., 2012).

Woodlands are critical for the moisture supply to the wetlands of northern Asia, Europe and Canada and some tropical wetlands in Sub-Saharan Africa and South America. The Crane, Maud, Plaines, Yenisei, Nigri, Pacaya, and Negro wetlands would be vulnerable to potential vegetation changes as the current moisture supply relies heavily on forests. These forests are now experiencing high deforestation rates, which could jeopardize, to some extent, such moisture supply. On the other hand, although Tibet and Sichuan wetlands have a large volume of precipitation from terrestrial sources, most comes from rangelands, which are already transformed by human activities, or at least the corresponding change in evaporation rates would not be as high as when forests are involved (Sterling et al., 2013).

In this sense, deforestation decreases evaporation, leading to positive feedbacks downwind (Staal et al., 2020; van der Ent, 2014). For instance, Staal et al. (2020) show the effect of deforestation on precipitation over the Amazon hydrological basin; a decrease in precipitation, mainly in the West of the hydrological basin, suggests that climate change seems to be the main driver of drying in the Amazon hydrological basin. Our study shows strong precipitation changes in the Amazon wetland basins, Negro and Pacaya but only little to no changes in the runoff in these basins (Sections 3.3 and 3.4).

This century is projected to see intense global population growth and urban and agricultural expansions, with the highest increases in tropical regions (Laurance et al., 2014). The expansion of rainfed agriculture can be associated with decreasing (Wang-Erlandsson et al., 2018) or increasing evaporation (Jaramillo et al., 2013),

depending on the original land cover and the regional hydroclimate. Our results suggest that rainfed agriculture expansions have already affected moisture supply to wetland hydrological basins in Canada, Africa, Asia, and Europe, and conversely, irrigation has affected some wetlands such as those in the Indus.

4.3. Limitations, Opportunities and Uncertainty

Wetland water availability is influenced by upwind moisture supply, climate variability and extremes (such as droughts, hurricanes and typhoons), anthropogenic climate change and anthropogenic pressures (e.g., infrastructure development, irrigation, flow regulation for energy, flood control, etc.). Differentiating these drivers is daunting due to the many drivers involved and the heterogeneity of wetlands worldwide (Åhlén et al., 2021; Ghajarnia et al., 2020; Thorslund et al., 2017). Several studies have tried to disentangle and separate individual drivers' effects; however, they have remained case-specific due to the reliance on limited data on wetland water availability (e.g., Buytaert & Beven, 2011; Gao et al., 2011; Hattermann et al., 2008). Therefore, combining our moisture tracking assessment, which considers upwind moisture supply, with these more in-situ effects into an overall vulnerability assessment, although convenient, is not yet possible at the spatial scales and variety of wetlands used in this study.

The two moisture tracking models, UTrack and WAM-2layers, which represent the state of the art, though are known to produce slightly different moisture source estimations. Presumably due to differences in the numerical methods and the vertical and spatial scales of the two models, mean annual terrestrial moisture recycling estimations by WAM2-layers, on average, exceed those estimated by UTrack by 5.4% ± 0.1% across the tropics (Cropper et al., 2021). For example, a comparison of country-scale mean annual terrestrial moisture recycling estimates between Dirmeyer et al. (2009) using the 3D-QIBT method and Link et al. (2020) using WAM-2layers shows, for example, a total difference of 20% for the Central African Republic, 28% for Paraguay and 2% for Portugal. Link et al. (2020) assume these differences could be caused by a false routing assumption in Dirmeyer et al. (2009), where too little land precipitation is routed to runoff and evaporates instead. Fully coupled Earth System Models (ESMs) also inherit such uncertainties, shown by differences in the estimation of precipitation across models (Aloysius et al., 2016) and in the divergence in their predictions of LUC impacts on precipitation (Pitman et al., 2012; Vetter et al., 2015). Studies like Harrington et al. (2023) use the Community Earth System Model to study regional moisture contributions to precipitation in North America and acknowledge that land moisture flows can be underestimated due to biases in the model's internal generation of evaporation. The moisture recycling community is now addressing such uncertainties between moisture tracking models, including ESMs, in a model intercomparison project initiated by Benedict et al. (2023) (for further Information, see: https://sites.google.com/view/imrrn/home).

In addition, studies have shown that different data inputs can lead to different moisture source estimations (e.g., Horan et al., 2023; Keys et al., 2014; Yang et al., 2023). In this study, the moisture source estimations (first two model runs) and the LUC impact could be over- or underestimated in certain basins, depending on the wet or dry bias in the underlying data input of the ERA5 reanalysis data and the STEAM—WAM-2layers coupling performed in Wang-Erlandsson et al. (2018). This could stem from known wet bias in ERA-Interim precipitation across the tropics, especially in Central Africa, and a dry bias over the continents in the Northern Hemisphere (Hassler & Lauer, 2021). Additionally, the first two model runs establishing the moisture sources of the wetland basins could include an overestimation in specific precipitation source areas, especially for the tropical basins (e.g., Ngiri, Negro) and those receiving moisture from Central Asia (e.g., Volga, Ili) due to a wet bias in the ERA5 reanalysis data. This is a challenge for many moisture recycling studies. For instance, Yang et al. (2023) studied the moisture sources of the Great Lakes Region in North America using the Dynamic Recycling Model, where they forced the model with different reanalysis data sets, namely North American Regional Reanalysis (NARR), MERRA-2, National Centers for Environmental Protection final analysis, and ERA5, compare the results with each other but also to observational precipitation and evaporation data sets. Their analysis shows that results from the forcing with NARR differ greatly from those obtained with the other three reanalysis datasets, leading them to suspect a water imbalance in the NARR data set. While the other three perform reasonably well, they find MERRA-2 to be the most consistent with observational data sets in the studied area. However, studies like Hassler and Lauer (2021) also find a 4% and 23% smaller bias in estimating precipitation across the tropics for ERA5 compared to MERRA-2 and JRA-55, respectively. The UTrack climatology is generated with ERA5 reanalysis data, and for consistency, we chose to use ERA5 evaporation and precipitation to establish the moisture sources and terrestrial recycling indices in this study. While confidence in ERA5 precipitation appears to be highest

outside the tropics, including Central Europe, China, and the South Asian Monsoon region (Hassler & Lauer, 2021; Jiao et al., 2021; Lavers et al., 2022), precipitation in the tropics although improved from ERA-Interim, still shows some errors, such as a wet bias and underestimations of low-intensity events (Gleixner et al., 2020; Lavers et al., 2022). Land evaporation in the ERA5 reanalysis data set can include overestimations across Central Asia, parts of the Middle East, Australia, and along the West Coast of South America in comparison to two other data sets (GLDAS2, MERRA-2) (Lu et al., 2021).

The contextual relevance of the conclusions may change in the context of climate change as moisture flows and atmospheric circulation undergo alterations, including an increasing importance of moisture flows from the oceans (Findell et al., 2019). Climate change can cause changes in atmospheric conditions (e.g., circulation changes). For example, the Hadley Circulation expansion has already been studied extensively (Hu et al., 2018), and a shift of the mid-latitude jets towards the poles is predicted under ongoing climate change (Osman et al., 2021). The atmospheric moisture flow data set used in this study is based on UTrack global computations and hourly atmospheric input data from 2008 to 2017 but is then aggregated to multi-annual monthly means and is also forced with averaged evaporation and precipitation data. Therefore, the potential effects of climate and LUC on local land-atmosphere coupling and atmospheric circulation are not addressed in this study. It is important to note that this study specifically considers the influence of LUC on precipitation, taking into consideration the effects of moisture recycling. Since average global annual moisture recycling estimates are predicted to decrease by 2%–3% per degree of global warming (Findell et al., 2019), our conclusions are likely to be also relevant under climate change.

The overall implications of downwind LUC on wetland water availability are still relevant, especially for assessing a general vulnerability of wetlands due to core moisture source regions, as Keys et al. (2014) established. Their core precipitationshed concept emphasizes the persistence of sources of evaporation. It reinforces the idea that because of the static moisture flows taken from the UTrack data set (Tuinenburg et al., 2020), differences in the input data (P, E) are just being translated proportionally to the magnitude of the difference. Therefore, we argue that studies, such as this one, combining static moisture trajectories with evaporation and precipitation data across various LUC scenarios, should be viewed as potential LUC impacts within the uncertainties of the applied data sets and scenario estimations. It is essential to recognize that the derived impacts are primarily linked back to downwind moisture recycling effects. We acknowledge that the STEAM—WAM-2layers data sets from Wang-Erlandsson et al. (2018) are generated with ERA-I atmospheric forcing data from 2000 to 2013 and land use classifications from 2005, which are not precisely the period of analysis used for the UTrack data set (2008–2017) and to develop the VI (1980–2020). However, interannual variability in moisture sources can mainly be traced back to a "pulsating" change in moisture source intensity within a core part of the precipitationshed (Keys et al., 2014), which leads us to contend that such a shift in the timeframe should not influence the results drastically.

5. Conclusion

We have assessed the vulnerability of the selected wetland basins to upwind LUC and accounted for the associated precipitation impacts through moisture recycling. For 30 of the 40 wetland hydrological basins, terrestrial sources contribute to at least half of the total annual precipitation. The lowest terrestrial precipitation recycling ratios are found in coastal wetland basins, where moisture mostly comes from the oceans. Although these wetland basins have a lower dependency on continental evaporation to sustain their precipitation, they still get at least 17%–23% of their total annual precipitation from land evaporation. Most precipitation in the sink regions comes from evaporation sources close to the sink but does not necessarily overlap with the sink area.

So far, the hydrological basins with the most substantial impact of land use changes on their precipitation and runoff are located in tropical and sub-tropical areas or where much land use has been converted to croplands. Water availability in all of these hydrological basins has been affected by changes in land use. As shown in the hydroclimatic trend analyses, many of the wetland hydrological basins are likely also affected by climatic change.

This study shows that wetlands in South America and Central Asia can be seen as vulnerable to the combined impacts of climatic changes and the effects of land use changes on their precipitation and runoff, here assumed as P–E. This is presented in the identified "hotspot" wetlands, where a decrease in runoff and precipitation caused by land use and climatic change can be observed.

This study highlights that land use changes outside basins can impact wetland basins' moisture recycling and precipitation patterns. Here, we show that precipitationshed analyses have the potential to contribute to a more complete understanding of drivers of wetland threats. However, more in-depth studies of such highlighted vulnerability hotspots using high-resolution time-series data of the source-to-sink moisture flows are needed to understand further wetland moisture recycling dynamics and, more broadly, all water-dependent ecosystems.

Data Availability Statement

All data used for this research are publicly available, and their sources are indicated and referenced in the Data section of this study. The wetland delineations can be accessed through the Ramsar Convention on Wetlands (2016) and Zhang et al. (2017). The digital elevation models for the basin delineations can be accessed through EU-DEM (European Environment Agency (EEA), 2015), SRTM (Jarvis et al., 2008), DEM3 (De Ferranti, 2011), and CDED (Canada's Natural Resources, 2015). Anthrome data can be accessed at Ellis et al. (2013). The hydrometeorological data (evaporation and precipitation) can be accessed through ERA5 Reanalysis (European Centre for Mid-Range Weather Forecasting (ECMWF), 2019; Hersbach et al., 2020), CRU-TSv4.5 (University of East Anglia Climatic Research Unit et al., 2021), UTrack moisture flow database (Tuinenburg et al., 2020). The STEAM evaporation and precipitation data from Wang-Erlandsson et al. (2018) can be accessed through Zenodo (Wang-Erlandsson et al., 2023). The figures and maps were generated using the Matplotlib library (Caswell et al., 2022), including the Basemap Matplotlib Toolkit and Cartopy to create 2D maps. The data sets of the Ramsar wetland basin delineations and the forward and backward atmospheric moisture flows generated in this research are available on Zenodo at Fahrländer et al. (2023). Finally, the Python scripts used for processing the moisture flows are available on GitHub under the MIT licence (https://github.com/sifa4152/utrack_dataset_wetland_processing.git).

Acknowledgments
The Baltic Sea Centre, Stockholm University and the Swedish Research Council (VR) Project 2021-05774 have funded this study. S.F.F. acknowledges financial support from the Netherlands Enterprise Agency (BG-Water Project and the "Global Commission on the Economics of Water"). L.W.-E. acknowledges financial support from Formas (Project "Governing atmospheric water flows," 2019-01220), the European Research Council (Project Earth Resilience in the Anthropocene, the ERC-2016-ADG 743080), and the IKEA foundation. F.J. acknowledges project 2022-01570 of the Swedish Research Council for Sustainable Development (FORMAS) and project 2021-05774 of the Swedish Research Council (VR). Finally, S.F.F. would like to thank Lauren Seaby Andersen for advice and feedback during the writing and review process.

References

Acreman, M. C., Fisher, J., Stratford, C. J., Mould, D. J., & Mountford, J. O. (2007). Hydrological science and wetland restoration: Some case studies from Europe. *Hydrology and Earth System Sciences*, *11*(1), 158–169. https://doi.org/10.5194/hess-11-158-2007

Åhlén, I., Vigouroux, G., Destouni, G., Pietroń, J., Ghajarnia, N., Anaya, J., et al. (2021). Hydro-climatic changes of wetlandscapes across the world. *Scientific Reports*, *11*(1), 2754. https://doi.org/10.1038/s41598-021-81137-3

Aloysius, N. R., Sheffield, J., Saiers, J. E., Li, H., & Wood, E. F. (2016). Evaluation of historical and future simulations of precipitation and temperature in central Africa from CMIP5 climate models. *Journal of Geophysical Research: Atmospheres*, *121*(1), 130–152. https://doi.org/10.1002/2015JD023656

Benedict, I., Weijenborg, C., & Keune, J. (2023). Moisture tracking community meeting - SPM3 at EGU23. In *EGU General Assembly 2023*. Retrieved from https://meetingorganizer.copernicus.org/EGU23/session/47466

Buytaert, W., & Beven, K. (2011). Models as multiple working hypotheses: Hydrological simulation of tropical alpine wetlands. *Hydrological Processes*, *25*(11), 1784–1799. https://doi.org/10.1002/hyp.7936

Canada's Natural Resources. (2015). Candian Digital Elevation Data (CDED) [Dataset]. Retrieved from https://open.canada.ca/data/en/dataset/7f245e4d-76c2-4caa-951a-45d1d2051333

Caswell, T. A., Lee, A., Droettboom, M., De Andrade, E. S., Hoffmann, T., Klymak, J., et al. (2022). matplotlib/matplotlib: REL: v3.6.1 (Version v3.6.1). *Zenodo*. https://doi.org/10.5281/ZENODO.7162185

Chaplin-Kramer, R., Neugarten, R. A., Sharp, R. P., Collins, P. M., Polasky, S., Hole, D., et al. (2022). Mapping the planet's critical natural assets. *Nature Ecology & Evolution*, *7*(1), 51–61. https://doi.org/10.1038/s41559-022-01934-5

Cropper, S., Solander, K., Newman, B. D., Tuinenburg, O. A., Staal, A., Theeuwen, J. J. E., & Xu, C. (2021). Comparing deuterium excess to large-scale precipitation recycling models in the tropics. *Npj Climate and Atmospheric Science*, *4*(1), 60. https://doi.org/10.1038/s41612-021-00217-3

Davidson, N. C. (2016). Wetland losses and the status of wetland-dependent species. In C. M. Finlayson, G. R. Milton, R. C. Prentice, & N. C. Davidson (Eds.), *The wetland book* (pp. 1–14). Springer Netherlands. https://doi.org/10.1007/978-94-007-6173-5_197-1

Davidson, N. C., van Dam, A. A., Finlayson, C. M., & McInnes, R. J. (2019). Worth of wetlands: Revised global monetary values of coastal and inland wetland ecosystem services. *Marine and Freshwater Research*, *70*(8), 1189. https://doi.org/10.1071/MF18391

De Ferranti, J. (2011). Digital elevation data [Dataset]. Retrieved from http://viewfinderpanoramas.org/dem3.html

Dirmeyer, P. A., Brubaker, K. L., & DelSole, T. (2009). Import and export of atmospheric water vapor between nations. *Journal of Hydrology*, *365*(1–2), 11–22. https://doi.org/10.1016/j.jhydrol.2008.11.016

Ellis, E. C., Goldewijk, K. K., & Siebert, S. (2013). Anthropogenic biomes of the world, Version 2: 2000 [Dataset]. NASA Socioeconomic Data and Applications Center (SEDAC). https://doi.org/10.7927/H4D798B9

Ellis, E. C., & Ramankutty, N. (2008). Putting people in the map: Anthropogenic biomes of the world. *Frontiers in Ecology and the Environment*, *6*(8), 439–447. https://doi.org/10.1890/070062

Eltahir, E. A. B., & Bras, R. L. (1996). Precipitation recycling. *Reviews of Geophysics*, *34*(3), 367–378. https://doi.org/10.1029/96RG01927

European Centre for Mid-Range Weather Forecasting (ECMWF). (2019). Climate Data Store (CDS) [Dataset]. Retrieved from https://cds.climate.copernicus.eu/cdsapp#!/dataset/reanalysis-era5-land-monthly-means?tab=overview

European Environment Agency (EEA). (2015). EU-DEM v1.1 (Version v1.1) [Dataset]. Retrieved from http://land.copernicus.eu/pan-european/satellite-derived-products/eu-dem/eu-dem-v1.1/view

Fahrländer, S. F., Wang-Erlandsson, L., Pranindita, A., & Jaramillo, F. (2023). Average monthly backward moisture footprints for 40 Ramsar wetland basins under potential and current vegetation scenarios (2008 - 2017) [Dataset]. Zenodo. https://doi.org/10.5281/ZENODO.7980604

Findell, K. L., Keys, P. W., Van Der Ent, R. J., Lintner, B. R., Berg, A., & Krasting, J. P. (2019). Rising temperatures increase importance of oceanic evaporation as a source for continental precipitation. *Journal of Climate*, *32*(22), 7713–7726. https://doi.org/10.1175/JCLI-D-19-0145.1

Fluet-Chouinard, E., Stocker, B. D., Zhang, Z., Malhotra, A., Melton, J. R., Poulter, B., et al. (2023). Extensive global wetland loss over the past three centuries. *Nature*, *614*(7947), 281–286. https://doi.org/10.1038/s41586-022-05572-6

Gao, H., Bohn, T. J., Podest, E., McDonald, K. C., & Lettenmaier, D. P. (2011). On the causes of the shrinking of Lake Chad. *Environmental Research Letters*, *6*(3), 034021. https://doi.org/10.1088/1748-9326/6/3/034021

Ghajarnia, N., Destouni, G., Thorslund, J., Kalantari, Z., Åhlén, I., Anaya-Acevedo, J. A., et al. (2020). Data for wetlandscapes and their changes around the world. *Earth System Science Data*, *12*(2), 1083–1100. https://doi.org/10.5194/essd-12-1083-2020

Gillies, et al. (2013). Rasterio: Geospatial raster I/O for {Python} programmers [Python]. *Mapbox*. Retrieved from https://github.com/rasterio/rasterio

Gleixner, S., Demissie, T., & Diro, G. T. (2020). Did ERA5 improve temperature and precipitation reanalysis over East Africa? *Atmosphere*, *11*(9), 996. https://doi.org/10.3390/atmos11090996

GRDC. (2020). *Major river basins of the world/Global Runoff Data Centre* (Version 2nd, rev. ext. ed.). Federal Institute of Hydrology (BfG).

Grill, G., Lehner, B., Thieme, M., Geenen, B., Tickner, D., Antonelli, F., et al. (2019). Mapping the world's free-flowing rivers. *Nature*, *569*(7755), 215–221. https://doi.org/10.1038/s41586-019-1111-9

Harrington, T. S., Nusbaumer, J., & Skinner, C. B. (2023). The contribution of local and remote transpiration, ground evaporation, and canopy evaporation to precipitation across North America. *Journal of Geophysical Research: Atmospheres*, *128*(7), e2022JD037290. https://doi.org/10.1029/2022JD037290

Harris, I., Osborn, T. J., Jones, P., & Lister, D. (2020). Version 4 of the CRU TS monthly high-resolution gridded multivariate climate dataset. *Scientific Data*, *7*(1), 109. https://doi.org/10.1038/s41597-020-0453-3

Hassler, B., & Lauer, A. (2021). Comparison of reanalysis and observational precipitation datasets including ERA5 and WFDE5. *Atmosphere*, *12*(11), 1462. https://doi.org/10.3390/atmos12111462

Hattermann, F. F., Krysanova, V., & Hesse, C. (2008). Modelling wetland processes in regional applications. *Hydrological Sciences Journal*, *53*(5), 1001–1012. https://doi.org/10.1623/hysj.53.5.1001

Hersbach, H., Bell, B., Berrisford, P., Hirahara, S., Horányi, A., Muñoz-Sabater, J., et al. (2020). The ERA5 global reanalysis. *Quarterly Journal of the Royal Meteorological Society*, *146*(730), 1999–2049. https://doi.org/10.1002/qj.3803

Horan, M. F., Batibeniz, F., Kucharski, F., Almazroui, M., Abid, M. A., Fu, J. S., & Ashfaq, M. (2023). Moisture sources for precipitation variability over the Arabian Peninsula. *Climate Dynamics*, *61*(9–10), 4793–4807. https://doi.org/10.1007/s00382-023-06762-2

Hu, Y., Huang, H., & Zhou, C. (2018). Widening and weakening of the Hadley circulation under global warming. *Science Bulletin*, *63*(10), 640–644. https://doi.org/10.1016/j.scib.2018.04.020

Jaramillo, F., Brown, I., Castellazzi, P., Espinosa, L., Guittard, A., Hong, S.-H., et al. (2018a). Assessment of hydrologic connectivity in an ungauged wetland with InSAR observations. *Environmental Research Letters*, *13*(2), 024003. https://doi.org/10.1088/1748-9326/aa9d23

Jaramillo, F., Desormeaux, A., Hedlund, J., Jawitz, J., Clerici, N., Piemontese, L., et al. (2019). Priorities and interactions of Sustainable Development Goals (SDGs) with focus on wetlands. *Water*, *11*(3), 619. https://doi.org/10.3390/w11030619

Jaramillo, F., & Destouni, G. (2014). Developing water change spectra and distinguishing change drivers worldwide. *Geophysical Research Letters*, *41*(23), 8377–8386. https://doi.org/10.1002/2014GL061848

Jaramillo, F., Licero, L., Åhlen, I., Manzoni, S., Rodríguez-Rodríguez, J. A., Guittard, A., et al. (2018b). Effects of hydroclimatic change and rehabilitation activities on salinity and mangroves in the Ciénaga Grande de Santa Marta, Colombia. *Wetlands*, *38*(4), 755–767. https://doi.org/10.1007/s13157-018-1024-7

Jaramillo, F., Prieto, C., Lyon, S. W., & Destouni, G. (2013). Multimethod assessment of evapotranspiration shifts due to non-irrigated agricultural development in Sweden. *Journal of Hydrology*, *484*, 55–62. https://doi.org/10.1016/j.jhydrol.2013.01.010

Jarvis, A., Reuter, H. I., Nelson, A., & Guevara, E. (2008). Hole-filled SRTM for the globe Version 4, available from the CGIAR-CSI SRTM 90m database [Dataset]. Retrieved from http://srtm.csi.cgiar.org

Jiao, D., Xu, N., Yang, F., & Xu, K. (2021). Evaluation of spatial-temporal variation performance of ERA5 precipitation data in China. *Scientific Reports*, *11*(1), 17956. https://doi.org/10.1038/s41598-021-97432-y

Kashaigili, J. J. (2008). Impacts of land-use and land-cover changes on flow regimes of the Usangu wetland and the Great Ruaha River, Tanzania. *Physics and Chemistry of the Earth, Parts A/B/C*, *33*(8–13), 640–647. https://doi.org/10.1016/j.pce.2008.06.014

Keys, P. W., Wang-Erlandsson, L., & Gordon, L. J. (2016). The precipitationshed as a tool for tracing hydrological tele-connections among social-ecological systems. In *EGU General Assembly 2016, EPSC2016-17709*. Retrieved from https://ui.adsabs.harvard.edu/abs/2016EGUGA..1817709K/abstract

Keys, P. W., Wang-Erlandsson, L., & Gordon, L. J. (2018). Megacity precipitationsheds reveal tele-connected water security challenges. *PLoS One*, *13*(3), e0194311. https://doi.org/10.1371/journal.pone.0194311

Keys, P. W., Barnes, E. A., van der Ent, R. J., & Gordon, L. J. (2014). Variability of moisture recycling using a precipitationshed framework. *Hydrology and Earth System Sciences*, *18*(10), 3937–3950. https://doi.org/10.5194/hess-18-3937-2014

Keys, P. W., van der Ent, R. J., Gordon, L. J., Hoff, H., Nikoli, R., & Savenije, H. H. G. (2012). Analyzing precipitationsheds to understand the vulnerability of rainfall dependent regions. *Biogeosciences*, *9*(2), 733–746. https://doi.org/10.5194/bg-9-733-2012

Keys, P. W., Wang-Erlandsson, L., Gordon, L. J., Galaz, V., & Ebbesson, J. (2017). Approaching moisture recycling governance. *Global Environmental Change*, *45*, 15–23. https://doi.org/10.1016/j.gloenvcha.2017.04.007

Laurance, W. F., Sayer, J., & Cassman, K. G. (2014). Agricultural expansion and its impacts on tropical nature. *Trends in Ecology & Evolution*, *29*(2), 107–116. https://doi.org/10.1016/j.tree.2013.12.001

Lavers, D. A., Simmons, A., Vamborg, F., & Rodwell, M. J. (2022). An evaluation of ERA5 precipitation for climate monitoring. *Quarterly Journal of the Royal Meteorological Society*, *148*(748), 3152–3165. https://doi.org/10.1002/qj.4351

Link, A., van der Ent, R., Berger, M., Eisner, S., & Finkbeiner, M. (2020). The fate of land evaporation – A global dataset. *Earth System Science Data*, *12*(3), 1897–1912. https://doi.org/10.5194/essd-12-1897-2020

Lu, J., Wang, G., Chen, T., Li, S., Hagan, D. F. T., Kattel, G., et al. (2021). A harmonized global land evaporation dataset from reanalysis products covering 1980–2017. https://doi.org/10.5194/essd-2021-61

Milton, S. J., & Siegfried, W. R. (1994). A conceptual model of arid rangeland degradation. *BioScience*, *44*(2), 70–76. https://doi.org/10.2307/1312204

Osland, M. J., Enwright, N. M., Day, R. H., Gabler, C. A., Stagg, C. L., & Grace, J. B. (2016). Beyond just sea-level rise: Considering macroclimatic drivers within coastal wetland vulnerability assessments to climate change. *Global Change Biology*, *22*(1), 1–11. https://doi.org/10.1111/gcb.13084

Osman, M. B., Coats, S., Das, S. B., McConnell, J. R., & Chellman, N. (2021). North Atlantic jet stream projections in the context of the past 1,250 years. *Proceedings of the National Academy of Sciences*, *118*(38), e2104105118. https://doi.org/10.1073/pnas.2104105118

Pitman, A. J., De Noblet-Ducoudré, N., Avila, F. B., Alexander, L. V., Boisier, J.-P., Brovkin, V., et al. (2012). Effects of land cover change on temperature and rainfall extremes in multi-model ensemble simulations. *Earth System Dynamics*, *3*(2), 213–231. https://doi.org/10.5194/esd-3-213-2012

Ramsar Convention on Wetlands. (2016). Ramsar Sites Information Service (RSIS) [Dataset]. Retrieved from https://rsis.ramsar.org/

Ramsar Convention on Wetlands. (2021). *Global Wetland Outlook: Special edition 2021*. Ramsar Convention Secretariat.

Rouault, E., Warmerdam, F., Schwehr, K., Kiselev, A., Butler, H., Łoskot, M., et al. (2022). GDAL (Version v3.4.2). *Zenodo*. https://doi.org/10.5281/ZENODO.5884351

Schulzweida, U. (2020). CDO user guide (Version 2.0.0). https://doi.org/10.5281/ZENODO.5614769

Staal, A., Flores, B. M., Aguiar, A. P. D., Bosmans, J. H. C., Fetzer, I., & Tuinenburg, O. A. (2020). Feedback between drought and deforestation in the Amazon. *Environmental Research Letters*, *15*(4), 044024. https://doi.org/10.1088/1748-9326/ab738e

Stagg, C. L., Osland, M. J., Moon, J. A., Hall, C. T., Feher, L. C., Jones, W. R., et al. (2019). Quantifying hydrologic controls on local- and landscape-scale indicators of coastal wetland loss. *Annals of Botany*, *125*(2), 365–376. https://doi.org/10.1093/aob/mcz144

Sterling, S. M., Ducharne, A., & Polcher, J. (2013). The impact of global land-cover change on the terrestrial water cycle. *Nature Climate Change*, *3*(4), 385–390. https://doi.org/10.1038/nclimate1690

Thorslund, J., Jarsjo, J., Jaramillo, F., Jawitz, J. W., Manzoni, S., Basu, N. B., et al. (2017). Wetlands as large-scale nature-based solutions: Status and challenges for research, engineering and management. *Ecological Engineering*, *108*, 489–497. https://doi.org/10.1016/j.ecoleng.2017.07.012

Tuinenburg, O. A., & Staal, A. (2020). Tracking the global flows of atmospheric moisture and associated uncertainties. *Hydrology and Earth System Sciences*, *24*(5), 2419–2435. https://doi.org/10.5194/hess-24-2419-2020

Tuinenburg, O. A., Theeuwen, J. J. E., & Staal, A. (2020). High-resolution global atmospheric moisture connections from evaporation to precipitation. *Earth System Science Data*, *12*(4), 3177–3188. https://doi.org/10.5194/essd-12-3177-2020

University of East Anglia Climatic Research Unit, Harris, I. C., Jones, P. D., & Osborn, T. (2021). *CRU TS4.05: Climatic Research Unit (CRU) Time-Series (TS) version 4.05 of high-resolution gridded data of month-by-month variation in climate (Jan. 1901- Dec. 2020)*. NERC EDS Centre for Environmental Data Analysis. Retrieved from https://catalogue.ceda.ac.uk/uuid/c26a65020a5e4b80b20018f148556681

van der Ent, R. J. (2014). *A new view on the hydrological cycle over continents*. Delft University of Technology, S.l.

van der Ent, R. J., & Savenije, H. H. G. (2011). Length and time scales of atmospheric moisture recycling. *Atmospheric Chemistry and Physics*, *11*(5), 1853–1863. https://doi.org/10.5194/acp-11-1853-2011

van der Ent, R. J., Savenije, H. H. G., Schaefli, B., & Steele-Dunne, S. C. (2010). Origin and fate of atmospheric moisture over continents. *Water Resources Research*, *46*(9), 2010WR009127. https://doi.org/10.1029/2010WR009127

van der Ent, R. J., Wang-Erlandsson, L., Keys, P., & Savenije, H. H. G. (2014). Contrasting roles of interception and transpiration in the hydrological cycle – Part 2: Moisture recycling. *Earth System Dynamics*, *5*(2), 471–489. https://doi.org/10.5194/esd-5-471-2014

Vetter, T., Huang, S., Aich, V., Yang, T., Wang, X., Krysanova, V., & Hattermann, F. (2015). Multi-model climate impact assessment and intercomparison for three large-scale river basins on three continents. *Earth System Dynamics*, *6*(1), 17–43. https://doi.org/10.5194/esd-6-17-2015

Wang, X., Wang, W., & Tong, C. (2016). A review on impact of typhoons and hurricanes on coastal wetland ecosystems. *Acta Ecologica Sinica*, *36*(1), 23–29. https://doi.org/10.1016/j.chnaes.2015.12.006

Wang-Erlandsson, L., Fetzer, I., Keys, P. W., van Der Ent, R. J., Savenije, H. H. G., & Gordon, L. J. (2018). Remote land use impacts on river flows through atmospheric teleconnections. *Hydrology and Earth System Sciences*, *22*(8), 4311–4328. https://doi.org/10.5194/hess-22-4311-2018

Wang-Erlandsson, L., Fetzer, I., Keys, P. W., van Der Ent, R. J., Savenije, H. H. G., & Gordon, L. J. (2023). STEAM evaporation and precipitation for potential vegetation and current land use scenarios (Version 1) [Dataset]. Zenodo. https://doi.org/10.5281/ZENODO.7983721

Wemple, B. C., Browning, T., Ziegler, A. D., Celi, J., Chun, K. P., Jaramillo, F., et al. (2018). Ecohydrological disturbances associated with roads: Current knowledge, research needs, and management concerns with reference to the tropics. *Ecohydrology*, *11*(3), e1881. https://doi.org/10.1002/eco.1881

Wine, M. L., & Davison, J. H. (2019). Untangling global change impacts on hydrological processes: Resisting climatization. *Hydrological Processes*, *33*(15), 2148–2155. https://doi.org/10.1002/hyp.13483

Woolway, R. I., Kraemer, B. M., Lenters, J. D., Merchant, C. J., O'Reilly, C. M., & Sharma, S. (2020). Global lake responses to climate change. *Nature Reviews Earth & Environment*, *1*(8), 388–403. https://doi.org/10.1038/s43017-020-0067-5

Xi, Y., Peng, S., Ciais, P., & Chen, Y. (2021). Future impacts of climate change on inland Ramsar wetlands. *Nature Climate Change*, *11*(1), 45–51. https://doi.org/10.1038/s41558-020-00942-2

Yang, Z., Qian, Y., Xue, P., Wang, J., Chakraborty, T. C., Pringle, W. J., et al. (2023). Moisture sources of precipitation in the Great Lakes Region: Climatology and recent changes. *Geophysical Research Letters*, *50*(5), e2022GL100682. https://doi.org/10.1029/2022GL100682

Zaki, N. A., Torabi Haghighi, A., Rossi, P. M., Tourian, M. J., Bakhshaee, A., & Klove, B. (2020). Evaluating impacts of irrigation and drought on river, groundwater and a terminal wetland in the Zayanderud Basin, Iran. In *Water*. MDPI. https://doi.org/10.3390/w12051302

Zhang, H. Y., Niu, Z. G., Xu, P. P., Chen, Y. F., Hu, S. J., & Gong, N. (2017). The boundaries and remote sensing classification datasets on large wetlands of international importance in 2001 and 2013. *Journal of Global Change Data & Discovery*, *1*(2), 230–238. https://doi.org/10.3974/geodp.2017.02.15

References From the Supporting Information

Kendall, M. G. (1975). *Rank correlation methods*. Oxford University Press.

Mann, H. B. (1945). Nonparametric tests against trend. *Econometrica*, *13*(3), 245. https://doi.org/10.2307/1907187

Ringard, J., Chiriaco, M., Bastin, S., & Habets, F. (2019). Recent trends in climate variability at the local scale using 40 years of observations: The case of the Paris region of France. *Atmospheric Chemistry and Physics*, *19*(20), 13129–13155. https://doi.org/10.5194/acp-19-13129-2019

Wang, F., Shao, W., Yu, H., Kan, G., He, X., Zhang, D., et al. (2020). Re-evaluation of the power of the Mann-Kendall test for detecting monotonic trends in hydrometeorological time series. *Frontiers in Earth Science*, *8*, 14. https://doi.org/10.3389/feart.2020.00014